Available online at www.sciencedirect.com
SCIENCE DIRECT®
Remote Sensing of Environment 90 (2004) 434–440
Remote Sensing of Environment
www.elsevier.com/locate/rse

Land surface temperature retrieval from LANDSAT TM 5

José A. Sobrino[a,*], Juan C. Jiménez-Muñoz[a], Leonardo Paolini[b]

[a] Global Change Unit, Department of Thermodynamics, Faculty of Physics, University of Valencia, Dr. Moliner 50, 46100 Burjassot, Spain
[b] Laboratorio de Investigaciones Ecológicas de las Yungas, Universidad Nacional de Tucumán, CC 34 (4107), Yerba Buena, Tucumán, Argentina

Received 30 July 2003; received in revised form 16 February 2004; accepted 20 February 2004

Abstract

In this paper, three methods to retrieve the land surface temperature (LST) from thermal infrared data supplied by band 6 of the Thematic Mapper (TM) sensor onboard the Landsat 5 satellite are compared. The first of them lies on the estimation of the land surface temperature from the radiative transfer equation using in situ radiosounding data. The others two are the mono-window algorithm developed by Qin et al. [International Journal of Remote Sensing 22 (2001) 3719] and the single-channel algorithm developed by Jiménez-Muñoz and Sobrino [Journal of Geophysical Research 108 (2003)]. The land surface emissivity (LSE) values needed in order to apply these methods have been estimated from a methodology that uses the visible and near infrared bands. Finally, we present a comparison between the LST measured in situ and the retrieved by the algorithms over an agricultural region of Spain (La Plana de Requena-Utiel). The results show a root mean square deviation (rmsd) of 0.009 for emissivity and lower than 1 K for land surface temperature when the Jiménez-Muñoz algorithm is used.

Keywords: Land surface temperature; LANDSAT TM 5; Emissivity

1. Introduction

Thematic Mapper (TM) data, sensor on board the Landsat 5 satellite, are one of the most used for environmental studies. TM is composed by seven bands, six of them in the visible and near infrared, and only one band located in the thermal infrared region. Band 1 (with central wavelength of 0.49 μm), in the following TM1, is used for coastal water studies, TM2 (0.56 μm) is used for crops identification and vegetation stage studies, TM3 and TM4 (0.66 and 0.83 μm, respectively) are used to calculate vegetation indexes, as the Normalized Difference Vegetation Index (NDVI), TM5 and TM7 (1.65 and 2.22 μm, respectively) can be used for clouds, ice, snow and geological formations discrimination, and finally band TM6 (with an effective wavelength of 11.457 μm) is used for Land Surface Temperature (LST) retrieval. The fact of possessing only one thermal band is an important limitation in order to obtain LST, it does not allow to apply a split-window method (Sobrino et al., 1996) neither a temperature/emissivity separation (TES) method (Gillespie et al., 1998) and therefore to obtain information about the emissivity spectrum of natural surfaces. For these reasons, band TM6 has not been used for environmental studies as the other bands have.

The main goal of this paper is therefore to show to the reader different procedures for retrieving LST from TM6 data in order to contribute to a more employment of this band in the future. To this end, three different single-channel methods will be analyzed: (i) the radiative transfer equation, (ii) Qin et al.'s algorithm, and (iii) Jiménez-Muñoz and Sobrino's algorithm. Once the methods are presented, a comparison has been made using a Landsat image acquired the 4th of July (at 10:00 GMT), in 1996, over the Requena-Utiel site (Valencia, Spain). This site is at 39.5°N and 1°W, and shows a great topographic and geologic homogeneity, with plains covered by crops (Boluda et al., 1988; Sánchez et al., 1984).

2. Land surface temperature retrieval

In this section, the three different methods mentioned above for retrieveing LST from the Landsat thermal channel will be presented.

2.1. Radiative transfer equation

The first of them is called as Radiative Transfer Equation (RTE), and the LST is obtained from the

* Corresponding author. Tel./fax: +34-96-354-31-15.
E-mail address: sobrino@uv.es (J.A. Sobrino).

0034-4257/$ - see front matter © 2004 Elsevier Inc. All rights reserved.
doi:10.1016/j.rse.2004.02.003

following expression of the RTE applied to the thermal infrared region:

$$L_{\text{sensor},\lambda} = \left[\varepsilon_\lambda B_\lambda(T_s) + (1-\varepsilon_\lambda)L^{\downarrow}_{\text{atm},\lambda}\right]\tau_\lambda + L^{\uparrow}_{\text{atm},\lambda} \quad (1)$$

where L_{sensor} is the at-sensor radiance or Top of Atmospheric (TOA) radiance, i.e., the radiance measured by the sensor, ε is the land surface emissivity, $B(T_s)$ is the blackbody radiance given by the Planck's law and T_s is the LST, $L^{\downarrow}_{\text{atm}}$ is the downwelling atmospheric radiance, τ is the total atmospheric transmissivity between the surface and the sensor and $L^{\downarrow}_{\text{atm}}$ is the upwelling atmospheric radiance. It should be noted that Eq. (1) depends on the wavelength considered, but also on the observation angle, although for Landsat, the nadir view provides good results. The atmospheric parameters τ, $L^{\downarrow}_{\text{atm}}$ and $L^{\downarrow}_{\text{atm}}$ can be calculated from in situ radiosoundings and using a radiative transfer codes like MODTRAN (Berk et al., 1989). Therefore, from Eq. (1) it is possible to find T_s by inversion of the Planck's law. Inversion of Eq. (1) can be interpreted as a correction of the atmospheric and the emissivity effects on the data measured by the sensor. The main constraint of this method is that needs in situ radiosounding launched simultaneously with the satellite passes.

2.2. The Qin et al.'s mono-window algorithm

In order to avoid the dependence on radiosounding in the RTE method, Qin et al. (2001) developed the following mono-window algorithm for obtaining LST from TM6:

$$T_s = \frac{1}{C}[a(1-C-D) + b(1-C-D)+C+D)T_{\text{sensor}} - DT_a] \quad (2)$$

with $C=\varepsilon\tau$, $D=(1-\tau)[1+(1-\varepsilon)\tau]$, $a=-67.355351$, $b=0.458606$, and where ε is the land surface emissivity, τ is the total atmospheric transmissivity, T_{sensor} is the at-sensor brightness temperature and T_a represents the mean atmospheric temperature given by

$$T_a = 16.0110 + 0.92621T_o \quad (3)$$

T_o being the near-surface air temperature. Qin et al. also estimate the atmospheric transmissivity from w, the atmospheric water vapor content, for the range 0.4–1.6 g/cm^2, according to

$$\tau = 0.974290 - 0.08007w \text{ (high } T_o) \quad (4a)$$

$$\tau = 0.982007 - 0.09611w \text{ (low } T_o) \quad (4b)$$

More details about this algorithm and its sensitivity can be found in the work of Qin et al. (2001).

2.3. The Jiménez-Muñoz and Sobrino's single-channel method

Finally, Jiménez-Muñoz and Sobrino (2003) have developed a generalized single-channel method in order to retrieve LST from only one thermal channel, in which the LST is given by the following equation:

$$T_s = \gamma\left[\varepsilon^{-1}(\psi_1 L_{\text{sensor}} + \psi_2) + \psi_3\right] + \delta \quad (5)$$

with

$$\gamma = \left\{\frac{c_2 L_{\text{sensor}}}{T^2_{\text{sensor}}}\left[\frac{\lambda^4}{c_1}L_{\text{sensor}} + \lambda^{-1}\right]\right\}^{-1} \quad (6a)$$

$$\delta = -\gamma L_{\text{sensor}} + T_{\text{sensor}} \quad (6b)$$

and where L_{sensor} is the at-sensor radiance in W m^{-2} sr^{-1} μm^{-1}, T_{sensor} is the at-sensor brightness temperature in K, λ is the effective wavelength (11.457 μm for band TM6), $c_1=1.19104\ 10^8$ W μm^4 m^{-2} sr^{-1} and $c_2=14387.7$ μm K. The atmospheric functions ψ_1, ψ_2 and ψ_3 can be obtained as a function of the total atmospheric water vapor content (w) according to the following equations particularized for TM6 data:

$$\psi_1 = 0.14714w^2 - 0.15583w + 1.1234 \quad (7a)$$

$$\psi_2 = -1.1836w^2 - 0.37607w - 0.52894 \quad (7b)$$

$$\psi_3 = -0.04554w^2 + 1.8719w - 0.39071. \quad (7c)$$

3. Land surface emissivity estimation from the NDVI method

The knowledge of land surface emissivity (LSE) is necessary to apply the above methods to a Landsat image. As it has been mentioned in the Section 1, the fact of possessing only one thermal channel makes impossible to apply well-known and accepted methods by the scientific community working in the thermal infrared, as for example the TES method (Gillespie et al., 1998). A possible alternative could be to obtain an LSE image from a classification image, in which an emissivity value for each class is assumed. However, this is not very operative because we need a good knowledge of the study area and emissivity measurements on the surfaces representatives of the different classes and coincident with the satellite overpasses (i.e., the vegetative cover of the agricultural areas could change with time).

An alternative, operative (easy to apply) procedure is to obtain the LSE image from the NDVI. Of the different approaches given in the literature (Sobrino & Raissouni, 2000; Valor & Caselles, 1996; Van de Griend & Owe, 1993), a modification of the last one has been used, the

NDVI Thresholds Method—$NDVI^{THM}$, which shows a good working in comparison to a reference method as the one based on the TISI indices (Becker & Li, 1990), as is pointed by Sobrino et al. (2001). The method proposed obtains the emissivity values from the NDVI considering different cases:

(a) NDVI < 0.2
In this case, the pixel is considered as bare soil and the emissivity is obtained from reflectivity values in the red region.

(b) NDVI>0.5
Pixels with NDVI values higher than 0.5 are considered as fully vegetated, and then a constant value for the emissivity is assumed, typically of 0.99. It should be noted that the samples considered in the paper are not included in cases (a) or (b).

(c) $0.2 \leq NDVI \leq 0.5$
In this case, the pixel is composed by a mixture of bare soil and vegetation, and the emissivity is calculated according to the following equation:

$$\varepsilon = \varepsilon_v P_v + \varepsilon_s (1 - P_v) + d\varepsilon \quad (8)$$

where ε_v is the vegetation of the emissivity and ε_s is the soil emissivity, P_v is the vegetation proportion obtained according to (Carlson & Ripley, 1997):

$$P_v = \left[\frac{NDVI - NDVI_{min}}{NDVI_{max} - NDVI_{min}} \right]^2 \quad (9)$$

where $NDVI_{max} = 0.5$ and $NDVI_{min} = 0.2$.

The term $d\varepsilon$ in Eq. (8) includes the effect of the geometrical distribution of the natural surfaces and also the internal reflections. For plain surfaces, this term is negligible, but for heterogeneous and rough surfaces, as forest, this term can reach a value of 2% (Sobrino, 1989). A good approximation for this term can be given by

$$d\varepsilon = (1 - \varepsilon_s)(1 - P_v) F \varepsilon_v \quad (10)$$

where F is a shape factor (Sobrino et al., 1990) whose mean value, assuming different geometrical distributions, is 0.55.

Taking into account Eqs. (8) and (10), the LSE can be obtained as:

$$\varepsilon = m\, P_v + n \quad (11)$$

with

$$m = \varepsilon_v - \varepsilon_s - (1 - \varepsilon_s) F \varepsilon_v \quad (12a)$$

$$n = \varepsilon_s + (1 - \varepsilon_s) F \varepsilon_v \quad (12b)$$

In order to apply this methodology, values of soil and vegetation emissivities are needed. To this end, a typical emissivity value of 0.99 for vegetation has been chosen. The choice of a typical value for soil is a more critical question, due to the higher emissivity values variation for soils in comparison with vegetation ones. A possible solution is to use the mean value for the emissivities of soils included in the ASTER spectral library (http://asterweb.jpl.nasa.gov) and filtered according to band TM6 filter function. In this way considering a total of 49 soils spectra, a mean value of 0.973 (with a standard deviation of 0.004) is obtained. Using these data (TM6 soil and vegetation emissivities of 0.97 and 0.99, respectively), the final expression for LSE is given by

$$\varepsilon_{TM6} = 0.004\, P_v + 0.986. \quad (13)$$

4. Atmospheric correction for bands TM3 and TM4: calculation of the NDVI

As has been commented in the previous section, the LSE can be retrieved from NDVI values. The data supplied by bands 3 and 4, located in the red and near infrared, respectively, can be used to construct this vegetation index according to the following equation:

$$NDVI = \frac{TM4 - TM3}{TM4 + TM3} \quad (14)$$

In a first approximation, it is possible to obtain NDVI values from at-sensor or TOA reflectivities, called as $NDVI_{TOA}$. However, it is more accurate to atmospherically correct the TOA values in order to obtain at-surface reflectivities and, in this way, estimate NDVI values more representative of the natural surfaces, called as $NDVI_{surf}$. As the NDVI is constructed from a normalized difference, low differences between $NDIV_{TOA}$ and $NDVI_{surf}$ are expected.

In this section, two different atmospheric correction methods and a comparison between the values obtained with them and the values obtained with regard to the $NDVI_{TOA}$ are shown.

4.1. Simplified method for atmospheric correction in the solar spectrum: SMAC

The SMAC method was developed by Rahman and Dedieu (1994). This algorithm converts the TOA reflectivity in at-surface reflectivity using some atmospheric data (as for example, water vapor, aerosols content, ozone, etc.) as input data. This method has been applied considering the atmospheric conditions presents at time of the Landsat image analyzed in this paper (i.e., water vapor = 1.181 g/cm^2, aerosol optical depth at 550 nm = 0.1 and ozone content = 0.3 atm cm). Thus, the following equations can be proposed (García, 1998):

$$\rho_{sup}^{TM3} = 1.0705 \rho_{TOA}^{TM3} - 0.0121 \quad (15a)$$

$$\rho_{sup}^{TM4} = 1.0805 \rho_{TOA}^{TM4} - 0.0047 \quad (15b)$$

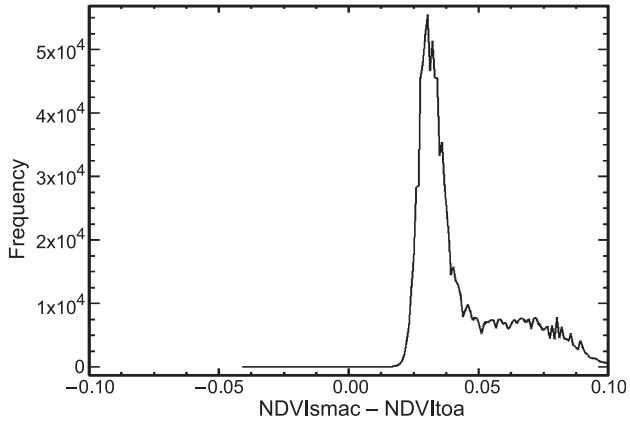

Fig. 1. Histogram for the image difference between the NDVI atmospherically corrected using the SMAC method (NDVIsmac) and the NDVI obtained without atmospheric correction (NDVItoa).

where ρ_{sup}^{TM3}, ρ_{sup}^{TM4} are the at-surface reflectivity and ρ_{TOA}^{TM3}, ρ_{TOA}^{TM4} are the TOA reflectivity for bands TM3 and TM4, respectively. Fig. 1 shows the histogram extracted from the image corresponding to the difference between $NDVI_{surf}$ corrected using the SMAC method and the $NDVI_{TOA}$. It is observed that the graph is centered around 0.03, which is not an important deviation.

4.2. Atmospheric correction based on image data

This method was developed by Chavez (1996), and its main advantage is that the data necessary in order to carry out the atmospheric correction are obtained from the image itself. For this purpose, the at-surface reflectivity is calculated with the following equation:

$$\rho_{sup} = \frac{\pi(L_{sat} - L_p)d^2}{E_o \cos\theta_z T_z} \tag{16}$$

where L_{sat} is the at-sensor radiance, T_z is the atmospheric transmissivity between the sun and the surface, θ_z is the zenithal solar angle, E_o is the spectral solar irradiance on the top of the atmosphere and d is the Earth–Sun distance and L_p is the radiance resulted from the interaction of the electromagnetic radiance with the atmospheric components (molecules and aerosols) that can be obtained according to:

$$L_p = L_{min} - L_{1\%} \tag{17}$$

where L_{min} is the radiance that corresponds to a digital count value for which the sum of all the pixels with digital counts lower or equal to this value is equal to the 0.01% of all the pixels from the image considered. The term $L_{1\%}$ is given by

$$L_{1\%} = \frac{0.01 \cos\theta_z T_z E_o}{\pi d^2} \tag{18}$$

with values for T_z of 0.85 and 0.91 for bands TM3 and TM4, respectively (Chavez, 1996). Fig. 2 shows the histogram corresponding to the difference between the $NDVI_{surf}$ obtained using this method and the $NDVI_{TOA}$. As in the previous case, the graph is centered at around 0.03. In Fig. 3, the histogram for the difference between the $NDVI_{surf}$ obtained using the atmospheric correction method SMAC and the $NDVI_{surf}$ obtained from the Chavez method is graphed. In this case, the histogram is centered at 0.0016, which is a negligible difference for NDVI values. Due to the similarity between both results, in the following, we will use the Chavez method because external data to the satellite is not needed.

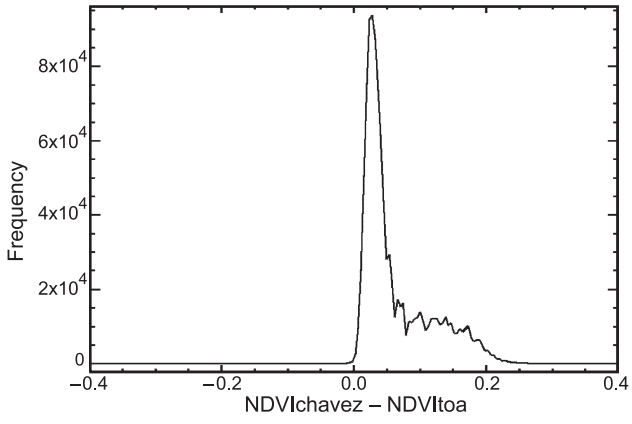

Fig. 2. Histogram for the image difference between the NDVI atmospherically corrected using the Chavez's method (NDVIchavez) and the NDVI obtained without atmospheric correction (NDVItoa).

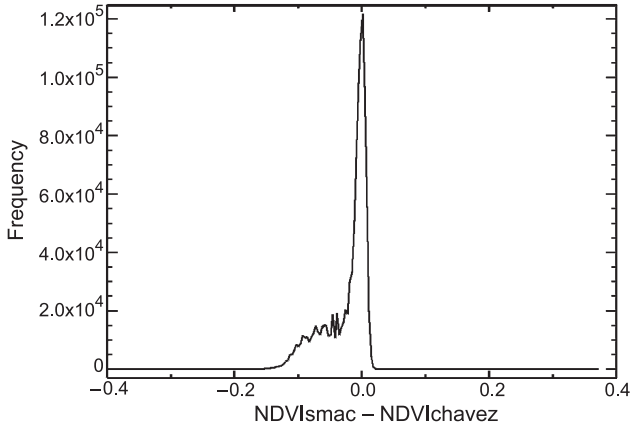

Fig. 3. Histogram for the image difference between the NDVI atmospherically corrected using the SMAC method (NDVIsmac) and the Chavez's method (NDVIchavez).

5. Results and discussion

In this section, we present the application of the methods given in Section 2 for retrieving LST such as the methodology presented in Section 3 for estimating LSE. To this end, a Landsat TM5 image acquired over the Requena-Utiel (Valencia, Spain) site was used. Finally, the results obtained

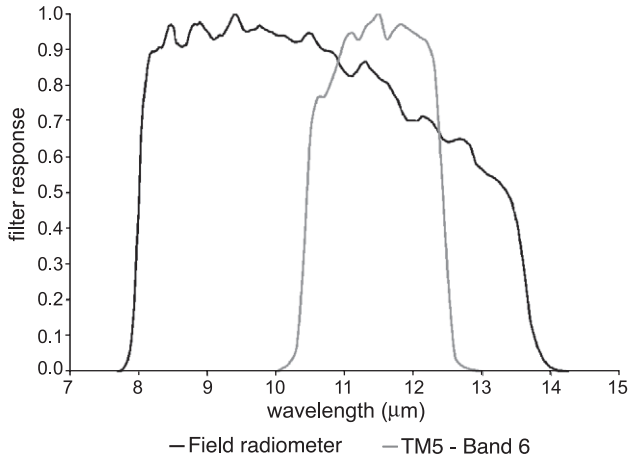

Fig. 4. Filter functions graph for the field radiometer CIMEL CE 312 band 1 (8–14 μm) and the Landsat TM 5 band 6 (10.4–12.5 μm).

for LSE and for LST (for the three methods considered) have been compared with in situ measurements.

5.1. Emissivity

The availability of in situ emissivity measurements using the box method (García, 1998; Nerry et al., 1998; Sobrino & Caselles, 1993) allow us to carry out a test of the results obtained using the NDVI method. For this purpose, Eq. (13) has been applied to the Landsat and the emissivity values have been extracted for those plots where the in situ emissivity measurements were made. It should be noted that in situ measurements were carried out with a RAYTEK ST8 radiometer with a single band in the range [8–14 μm], whereas band TM6 is located in the range [10.40–12.50 μm] (see Fig. 4, in which the filter function corresponding to the CIMEL broadband 8–14 μm is represented, so the filter function for the RAYTEK ST8 radiometer is not available). Due to these differences, in order to compare emissivity values obtained with Eq. (13) from TM6 data with emissivity values measured in situ, it is necessary to correct these last and transform them in TM6 values. For vegetation plots, this transformation is not necessary because the vegetation spectra show low spectral variations. However, this correction is necessary for soil plots. For this purpose, the ASTER spectral library is used again. A mean difference of 0.02 between the soils emissivities values obtained using the TM6 filter and the 8–14-μm filter of 0.02 is obtained. Table 1 shows the in situ emissivity values and the adapted to TM6 characteristics. From the comparison between these values and the ones given in Eq. (13), a root mean square deviation (rmsd) value of 0.009 is obtained. Although this methodology provides good results (rmsd = 0.1), it should be noticed that cannot be applied to non-vegetated surfaces with high emissivity values (as water, ice and snow). In these situations, the usual procedure is to identify this pixels in the Landsat image and assume the emissivity values published in the literature.

Table 1
Comparison between the emissivity measured in situ and the emissivity obtained from the NDVI method

Plot	NDVI	$\varepsilon_{\text{in situ}}^{\text{TM6}}$	$\varepsilon_{\text{NDVI}}$	$\varepsilon_{\text{in situ}}^{\text{TM6}} - \varepsilon_{\text{NDVI}}$
Reddish soil and vine	0.26	0.994 (0.974)	0.986	0.008
Light soil, few vegetation	0.34	0.968 (0.948)	0.987	−0.019
Brown soil	0.26	0.982 (0.962)	0.986	−0.004
Vine	0.32	0.990 (0.990)	0.987	0.003
Mixed soil (brown and light)	0.31	0.987 (0.967)	0.987	0.000
Clayish soil	0.34	0.986 (0.966)	0.987	−0.001
Forest	0.55	0.984 (0.984)	0.990	−0.006
			bias	−0.003
			σ	0.008
			rmsd	0.009

In parentheses, the emissivity measured in situ with the RAYTEK radiometer in the range [8–14 μm]. The bias, standard deviation (σ) and root mean square deviation (rmsd) values are also included.

Table 2
Comparison between the "in situ" land surface temperature and the obtained from the RTE using the radiosounding data and the emissivity obtained from the NDVI methodology

Plot	$T_s^{\text{in situ}}$ (K)	T_s^{RTE} (K)	$T_s^{\text{in situ}} - T_s^{\text{RTE}}$ (K)
Reddish soil and vine	311.88	312.40	−0.51
Light soil, few vegetation	311.66	310.44	1.22
Brown soil	312.55	312.29	0.26
Vine	311.15	311.34	−0.19
Mixed soil (brown and light)	313.19	313.19	0.00
Clayish soil	312.90	312.84	0.06
Forest	306.24	305.88	0.36
		bias	0.17
		σ	0.54
		rmsd	0.57

5.2. Temperature

In order to test the LST obtained with the different methods proposed in the paper, values measured in situ are needed. Unfortunately, these data are not available. However, the radiosounding launched near the study area at 12:00 GMT including altitude, pressure, temperature and humidity

Table 3
Comparison between the "in situ" land surface temperature and the obtained from the Qin et al.'s algorithm using the emissivity obtained from the NDVI methodology

Plot	$T_s^{\text{in situ}}$ (K)	$T_s^{\text{Qin et al.}}$ (K)	$T_s^{\text{in situ}} - T_s^{\text{Qin et al.}}$ (K)
Reddish soil and vine	311.88	310.44	−1.44
Light soil, few vegetation	311.66	308.56	−3.10
Brown soil	312.55	310.34	−2.21
Vine	311.15	309.42	−1.73
Mixed soil (brown and light)	313.19	311.20	−1.99
Clayish soil	312.90	310.86	−2.04
Forest	306.24	304.17	−2.08
		bias	−2.09
		σ	0.52
		rmsd	2.15

Table 4
Comparison between the "in situ" land surface temperature and the one obtained with the Jiménez-Muñoz and Sobrino's algorithm (JM&S) using the emissivity obtained from the NDVI methodology

Plot	$T_s^{\text{in situ}}$ (K)	$T_s^{\text{JM\&S}}$ (K)	$T_s^{\text{in situ}} - T_s^{\text{JM\&S}}$ (K)
Reddish soil and vine	311.88	313.28	− 1.39
Light soil, few vegetation	311.66	311.44	0.22
Brown soil	312.55	313.18	− 0.63
Vine	311.15	312.28	− 1.14
Mixed soil (brown and light)	313.19	314.02	− 0.82
Clayish soil	312.90	313.68	− 0.78
Forest	306.24	307.17	− 0.93
		bias	− 0.78
		σ	0.51
		rmsd	0.93

profiles allow us to estimate the transmissivity and atmospheric radiances by means of the MODTRAN 3.5 code (Abreu & Anderson, 1996). From radiosounding data, in situ emissivity and at-sensor radiances extracted from the Landsat image, it is possible to obtain the LST using Eq. (1) by inversion of the Planck's law. It should be noted that assuming the calibration of the sensor, the obtained and measured LST must be similar. Table 2 shows the test for the LST retrieved from the RTE using the LSE estimated with the NDVI method, an rmsd value less than 0.6 K is obtained, which is due to the indetermination of the emissivity.

In order to validate the Qin et al.'s algorithm, the temperature corresponding to the first level of the radiosounding has been chosen as air temperature, $T_o = 302.55$ K, and the mean atmospheric temperature has been calculated using Eq. (3). The atmospheric water vapor content is 1.181 g/cm^2 from the radiosounding data. It is difficult to classify the T_o value into 'low' (Eq. (4a)) or 'high' (Eq. (4b)), so the atmospheric transmissivity has been calculated using both equations, and then the mean value has been considered. The result is given in Table 3, which shows an rmsd value of 2.2 K when the LSE is obtained using the NDVI method and 1.9 K when we used the LSE measured in situ. It should be noted that better result, an rmsd of 0.9 K, is obtained when we used Eq. (2) instead of the approximations involved in Eqs. (3), (4a) and (4b). This illustrates the fact that the Qin et al.'s algorithm provides accurate results when input parameters are adequate.

Table 5
Root mean square deviation values (in K) of the comparison between the LST measured in situ and the obtained for the algorithms discussed in the paper when different input data are considered

Algorithm	Input data used to retrieve the LST			
	Radiosounding emissivity in situ	Radiosounding emissivity $NDVI^{THM}$	Water vapor emissivity in situ	Water vapor emissivity $NDVI^{THM}$
RTE	0.0	0.6	Not applicable	Not applicable
Qin et al.	0.9	0.9	1.9	2.2
JM&S	Not applicable	Not applicable	1.0	0.9

Table 6
Same as Table 5, but extracting average values of a sample composed by 9×9 pixels from the Landsat image

Algorithm	Input data used to retrieve the LST			
	Radiosounding emissivity in situ	Radiosounding emissivity $NDVI^{THM}$	Water vapor emissivity in situ	Water vapor emissivity $NDVI^{THM}$
RTE	0.0	0.6	Not applicable	Not applicable
Qin et al.	0.5	0.6	2.4	2.6
JM&S	Not applicable	Not applicable	0.5	0.6

Finally, Table 4 shows the test for the Jiménez-Muñoz and Sobrino's method using the LSE obtained from NDVI. Here an rmsd less than 1 K is obtained. In comparison with the Qin et al.'s algorithm, this is due to the improvement in the bias value. In this case, the use of the in situ emissivities measurements does not improve the result, the same rmsd value is obtained.

Finally, we summarizes in Table 5 the results obtained for the different algorithms and inputs. The best result is obtained when the RTE is used, an rmsd value of 0.6 K. In the same conditions, i.e., when radiosounding data is used, the Qin et al.'s algorithm provides an rmsd value of 0.9 K. However, when radiosounding data are not available, the RTE is not applicable, and only the Qin et al.'s and the Jiménez-Muñoz and Sobrino's algorithms can be applied. In this case, an rsmd value of 2 and 1 K is obtained, respectively. So, in this particular situation, the Jiménez-Muñoz and Sobrino's algorithm seems to improve the results, with the additional advantage that in this algorithm the knowledge of air temperature is not necessary.

5.3. Average effects

The results showed in the previous sections have been obtained using individual measurements, i.e., the algorithms have not been applied to the Landsat image. Another possibility is to apply the equations to a Landsat image, and then to extract the mean value for a given sample composed by a certain number of pixels. In Table 6, we show the rmsd values obtained for a region composed by 9×9 pixels for the three LST algorithms considered in this paper. This tables shows that the average procedure produces a decrease of approximately 0.5 K in the rmsd, except in the cases of applying RTE and the Qin et al.'s algorithm when water vapor content is used as input data.

6. Conclusions

In this paper, three different methods in order to retrieve LST from known LSE values or LSE values obtained with the NDVI method have been presented. The first of them consist on applying the radiative transfer equation from radiosounding data and a radiative transfer code as MOD-

TRAN, whereas the two others consist on single-channel algorithms. One of them, developed by Qin et al. (2001), uses the atmospheric water vapor and the near-surface air temperature for retrieving the LST, whereas the other one, developed by Jiménez-Muñoz and Sobrino (2003), uses only the atmospheric water vapor content. The test of these algorithms has been carried out from a Landsat TM 5 image acquired the 4th of July, in 1996, over the Requena-Utiel (Valencia, Spain) site. Emissivity measured in situ and a radiosounding have been also used in order to reproduce the in situ LST. The LST retrieved using the radiative transfer equation, which is only applicable when an in situ radiosounding is available, shows an rmsd value of 0.6 K when the LSE obtained with the NDVI method is considered. The Qin et al.'s and Jiménez-Muñoz and Sobrino's algorithms, which not need an in situ radiosounding, show rmsd values of 2 and 0.9 K, respectively. Best results are obtained with the Qin et al.'s algorithm when the radiosounding data is used, with an rmsd of 0.9 K. The average effect involved when the values are extracted from the satellite image has been also analyzed. When samples of 9×9 pixels are considered, the average procedure shows an improvement of 0.5 K approximately. In this case, despite of the Landsat constrain of possessing only one thermal channel, it is possible to obtain an rmsd value lower than 0.6 K using the Jiménez-Muñoz and Sobrino's algorithm.

Acknowledgements

We wish to thank the European Union (project WATERMED ICA3-ct-1999-00015) and the Ministerio de Ciencia y Tecnología (project REN2001-3105/CLI) for the financial support. We also wish to thank R. Boluda for providing us with the Landsat image. P. Sobrino, A. García and N. Raissouni are acknowledged for the field measurements.

References

Abreu, L. W., & Anderson, G. P. (Eds.) (1996). *The MODTRAN 2/3 Report and LOWTRAN 7 MODEL*, Modtran Report, Contract F19628-91-C-0132, Philips Laboratory.

Becker, F., & Li, Z. -L. (1990). Temperature independent spectral indices in thermal infrared bands. *Remote Sensing of Environment*, *32*, 17–33.

Berk, A., Bernstein, L. S., & Robertson, D. C. 1989. *MODTRAN: A Moderate Resolution Model for LOWTRAN 7*, Technical Report GL-TR-89-0122, Geophys. Lab, Bedford, MA.

Boluda, R., Andreu, V., Moraleda, M., & Sánchez, J. (1988). Factores ecológicos (geología, vegetación y clima) de la Comarca de La Plana de Requena-Utiel (Valencia). Vegetación y clima. *Anales de Edafología y Agrobiología*, *XLVII*(5–6), 903–917.

Carlson, T. N., & Ripley, D. A. (1997). On the relation between NDVI, fractional vegetation cover, and leaf area index. *Remote Sensing of Environment*, *62*, 241–252.

Chavez, P. S. (1996). Image-based atmospheric correction—revisited and improved. *Photogrammetric Engineering and Remote Sensing*, *62*(9), 1025–1036.

García, A. J. (1998). *Corrección atmosférica de imágenes Landsat-5 Thematic Mapper. Aplicación al estudio de la comarca de Requena-Utiel*, degree dissertation, Politecnic University of Valencia, Valencia, Spain, 217 pp.

Gillespie, A. R., Rokugawa, S., Hook, S., Matsunaga, T., & Kahle, A. B. (1998). A temperature and emissivity separation algorithm for Advanced Spaceborne Thermal Emission and Reflection Radiometer (ASTER) images. *IEEE Transactions on Geoscience and Remote Sensing*, *36*, 1113–1126.

Jiménez-Muñoz, J. C., & Sobrino, J. A. (2003). A generalized single-channel method for retrieving land surface temperature from remote sensing data. *Journal of Geophysical Research*, *108* (doi: 10.1029/2003JD003480).

Nerry, F., Labed, J., & Stoll, M. P. (1998). Emissivity signatures in the thermal IR band for Remote Sensing: calibration procedure and method of measurement. *Applied Optics*, *27*, 758–764.

Qin, Z., Karnieli, A., & Berliner, P. (2001). A mono-window algorithm for retrieving land surface temperature from Landsat TM data and its application to the Israel–Egypt border region. *International Journal of Remote Sensing*, *22*(18), 3719–3746.

Rahman, H., & Dedieu, G. (1994). SMAC: A simplified method for the atmospheric correction of satellite measurements in the solar spectrum. *International Journal of Remote Sensing*, *15*, 123–143.

Sánchez, J., Rubio, J.L., Salvador, P., & Arnal, S. (1984). *Metodología de la Cartografía Básica, I Congreso Español de Geología, Segovia, Spain* (pp. 771–782). Madrid Ilustre Colegio Oficial de Geólogos.

Sobrino, J. A. (1989). *Desarrollo de un modelo teórico para implementar la medida de la temperatura realizada mediante teledetección. Aplicación a un campo de naranjos*, PhD dissertation, University of Valencia, Valencia, Spain, 170 pp.

Sobrino, J. A., & Caselles, V. (1993). A field method for estimating the thermal infrared emissivity. *ISPRS Journal of Photogrammetry and Remote Sensing*, *48*, 24–31.

Sobrino, J. A., Caselles, V., & Becker, F. (1990). Significance of the remotely sensed thermal infrared measurements obtained over a citrus orchard. *ISPRS Photogrammetric Engineering and Remote Sensing*, *44*, 343–354.

Sobrino, J. A., Li, Z. L., Stoll, M. P., & Becker, F. (1996). Multi-channel and multi-angle algorithms for estimating sea and land surface temperature with ATSR data. *International Journal of Remote Sensing*, *17*(11), 2089–2114.

Sobrino, J. A., & Raissouni, N. (2000). Toward remote sensing methods for land cover dynamic monitoring. Application to Morocco. *International Journal of Remote Sensing*, *21*, 353–366.

Sobrino, J. A., Raissouni, N., & Li, Z. -L. (2001). A comparative study of land surface emissivity retrieval from NOAA data. *Remote Sensing of Environment*, *75*, 256–266.

Valor, E., & Caselles, V. (1996). Mapping land surface emissivity from NDVI: application to European, African and South American areas. *Remote Sensing of Environment*, *57*, 167–184.

Van de Griend, A. A., & Owe, M. (1993). On the relationship between thermal emissivity and the normalized difference vegetation index for natural surfaces. *International Journal of Remote Sensing*, *14*(6), 1119–1131.